Asian Journal of Chemistry; Vol. 26, No. 15 (2014), 4759-4766

ASIAN JOURNAL OF CHEMISTRY

http://dx.doi.org/10.14233/ajchem.2014.16199

Activity and Selectivity of Cu and Ni Doped TiO_2 in the Photocatalytic Reduction of CO_2 with H_2O Under UV-light Irradiation

Z.Q. He, L.X. Jiang, J. Han, L.N. Wen, J.M. Chen and S. Song*

College of Biological and Environmental Engineering, Zhejiang University of Technology, Hangzhou 310032, P.R. China

*Corresponding author: Tel/Fax: +86 571 88320276, E-mail: ss@zjut.edu.cn

Received: 17 August 2013; *Accepted*: 10 December 2013; *Published online*: 16 July 2014; AJC-15567

Photocatalysis has been found to be an effective method to convert CO_2 into valuable products. To explore the selectivity and photocatalytic activity of transition metal doped TiO_2 catalysts for the reduction of CO_2, a series of Cu and Ni (0.5-7.0 wt. %) doped TiO_2 nanoparticles were prepared by means of a hydrolysis method. Photocatalytic experiments were conducted under irradiation from Hg lamps in a CO_2/NaOH aqueous solution. The results indicate that the photoreduction of CO_2 with water, catalyzed by Cu-TiO_2 and Ni-TiO_2, can yield CO, HCHO, CH_3OH and CH_4. Methane was identified as the major products using Cu-TiO_2 or Ni-TiO_2. In addition, Ni-TiO_2 shows greater CO_2 conversion in comparison with Cu-TiO_2. With the help of X-ray diffraction, X-ray photoelectron spectroscopy, Brunauer-Emmett-Teller measurements, transmission electron microscopy and UV-visible absorption spectra, it is concluded that both the adsorption and dissociation of CO_2 and improvement of the photocatalytic activity by forming a n-p junction and providing matching band potentials, play a crucial role in determining the types and amounts of photoproducts.

Keywords: Photocatalytic reduction, Carbon dioxide, Cu doped TiO_2, Ni doped TiO_2, Heterojunction.

INTRODUCTION

The conversion of CO_2 into useful materials, such as CO, HCHO, CH_3COOH, CH_3OH and CH_4, is considered to be one of the best ways to solve issues of global warming and energy shortages[1,2]. However, the activation of CO_2, to form high-potential carbon compounds, requires a thermodynamic energy increase of about 220-330 kJ/mol[3,4]. Consequently, reduction of CO_2 always requires extreme conditions, including high pressure or high temperature or both.

To date, the photoreduction method has been regarded as the most promising approach, since solar energy is the ultimate and inexhaustible source of energy on earth[5]. In view of the fact that the reduction potential for the conversion of CO_2 to CH_4 is -0.24 V (*vs*. NHE)[6], TiO_2 with a conduction band (CB) energy of -0.29 eV, is considered to be an appropriate candidate for this photocatalyic process[7]. However, the disadvantages of the wide band gap of TiO_2 (3.2 eV for anatase) and the high recombination rate of the photogenerated electron-hole pairs greatly hinders the CO_2 conversion efficiency[8,9]. Doping TiO_2 with metals (*e.g*. Pt, Ag, Ru, Rh, Au, Cu, Ni, *etc*.) or nonmetals (*e.g*. C, N, S, I, *etc*.) might be an effective way to overcome these drawbacks[10-19]. However, previous work has focused mainly on the preparation of new catalysts to improve the photocatalytic activity of CO_2. Sometimes, close attention is paid to only one particular photoproduct and few reports have focused on the selectivity of the photoproduct and the photocatalytic activity of different photocatalysts under similar conditions.

In comparison to other metal dopants, Cu and Ni, as representatives of group IB and VIII might be able to dissociate adsorbed CO_2[20-22]. This might then promote mass transfer of CO_2 from the liquid phase to the catalyst surface, facilitating CO_2 activation and reduction. For this reason, Cu and Ni were selected as candidates to compare the activity and selectivity of doped TiO_2 photocatalysts.

The Cu-TiO_2 and Ni-TiO_2 catalysts, doped with different concentrations of the metal, were synthesized using the hydrolysis method. Their photocatalytic properties were then compared by reducing CO_2 in alkaline solution. Systematic characterization by methods that included X-ray diffraction (XRD), X-ray photoelectron spectroscopy (XPS), the Brunauer-Emmett-Teller (BET) measurement, transmission electron microscopy (TEM) and UV-visible absorption spectra, were used to elucidate the relationship between the structure and the photoproperties, including activity and selectivity, of the photocatalysts.

EXPERIMENTAL

All chemicals were of analytical grade or higher and were used as received. Carbon dioxide (purity 99.999 %) was

provided by Hangzhou Jingong Special Gas Co., Ltd., China. $Cu(NO_3)_2{\cdot}3H_2O$, $Ni(NO_3)_2{\cdot}6H_2O$, CH_3COOH and tetrabutyl titanate [$Ti(OBu)_4$], used for the preparation of photocatalysts, were obtained from Huadong Medicine Co., China. The other reagents used in this work, such as NaOH, ammonium acetate (CH_3COONH_4) and acetylacetone ($CH_3COCH_2COCH_3$) were purchased from Shanghai Jingchun Reagent Co., China. Deionized water (18 MΩ) was used for all solutions.

Preparation of catalysts: The Cu-TiO_2 catalysts were prepared as follows. A measured amount of $Cu(NO_3)_2{\cdot}3H_2O$ was dissolved in 100 mL deionized water and the pH value of the aqueous solution was adjusted to 2.5 using CH_3COOH. Next, 21 mL of $Ti(OBu)_4$ was added dropwise to the mixture with continuous stirring. After vigorous stirring for 3 h, the mixture was dried at 80 °C overnight in air. The resulting product was calcined in an oven (CWF1100, CARBOLITE, England). The temperature was raised at a rate of 5 °C/min from room temperature to 450 °C and held at this temperature for 2 h, followed by cooling naturally to room temperature. Various Ni-doped TiO_2 powders were prepared in a similar way.

Characterization of the catalysts: A structural analysis of the catalysts was carried out by XRD with a Thermo ARL SCINTAG X'TRA diffractometer at room temperature, using CuK_α irradiation at 45 kV and 40 mA. The XPS analysis of the samples was performed on a RBD upgraded PHI-5000C ESCA system (Perkin-Elmer) with MgK_α radiation (1253.6 eV) and all the binding energies were calibrated with reference to the C1s peak at 284.6 eV. The TEM micrographs were examined using a Tecnai G2 F30 S-Twin microscope operating at 300 kV and 0.2 nm point resolution. Specific surface areas (S_{BET}) of the samples were determined using the BET method with a Micromeritics ASAP 2010 analyser by measurement of the nitrogen adsorption-desorption isotherm at 77 K. UV-visible absorption spectra of samples were determined on a Spectro UV-2550 instrument at room temperature with $BaSO_4$ as a reference.

Photocatalytic reactions: The photoreduction of CO_2 was carried out in a quartz reactor (diameter 4.5 cm, height 22 cm, total capacity 350 mL) containing 300 mL of 0.2 M NaOH and 0.3 g of the photocatalyst, surrounded by two 18 W low pressure mercury lamps (Beijing Electric Light Sources Research Institute, Beijing, China) as UV light source. These have an emission spectrum peaking at 254 nm. The suspension was irradiated whilst stirring and samples were withdrawn through a port at the top of the reactor. The temperature of the reaction system was maintained at 35 °C. The reason why NaOH aqueous solution was employed as the solvent is because NaOH not only acts as a strong hole-scavenger, reducing the recombination of hole-electron pairs, but also as a solvent, enhancing the solubility of CO_2 in the liquid phase[23].

Prior to the UV illumination, CO_2 was bubbled through the reactor at a constant rate for at least 0.5 h to eliminate air and saturate the solution. For each run, samples were collected from the gas and liquid phases at preset times. The liquid samples were centrifuged and passed through a 0.45 μm pore size membrane to remove any suspended solids.

Sample analysis: H_2 and CO in the gas phase were quantified using a gas chromatograph (GC 6890 N, Agilent Technologies, USA) equipped with TCD detector and an HP-PLOT MOLESIEVE capillary column (30 m × 320 μm × 12 μm). CH_4 was analyzed using a gas chromatograph (GC-2014, Shimadzu, Japan) equipped with a FID detector and RTX-1701 column (30 m × 250 μm × 25 μm).

Formaldehyde in aqueous solution was determined *via* the acetylacetone spectrophotometric method using a UV-visible spectrophotometer (T6, Beijing Puxi General Instrument Co., China). CH_3OH was detected using a gas chromatograph (GC 6890 N, Agilent, USA) equipped with a FID detector and an HP-INNOWAX capillary column (30 m × 320 μm × 25 μm)[24]. Note that HCOOH cannot be detected using an ionic chromatograph (ICS2000, Dionex, USA) below a detection limit of 0.2 μmol/L.

RESULTS AND DISCUSSION

Catalyst characterization: Fig. 1 shows the XRD diffraction patterns of Cu-TiO_2 and Ni-TiO_2 catalysts with different metal contents (0.5-7.0 wt. %). All Cu-TiO_2 and Ni-TiO_2 samples exhibited clear well-crystallized anatase phases, with peaks at 2θ values 25.2°, 37.9°, 48.3°, 53.9°, 55.0°, 62.7°, 68.9°, 70.1° and 75.5°. These can be assigned to the (101), (004), (200), (105), (211), (204), (116), (220) and (215) crystal planes of anatase TiO_2.

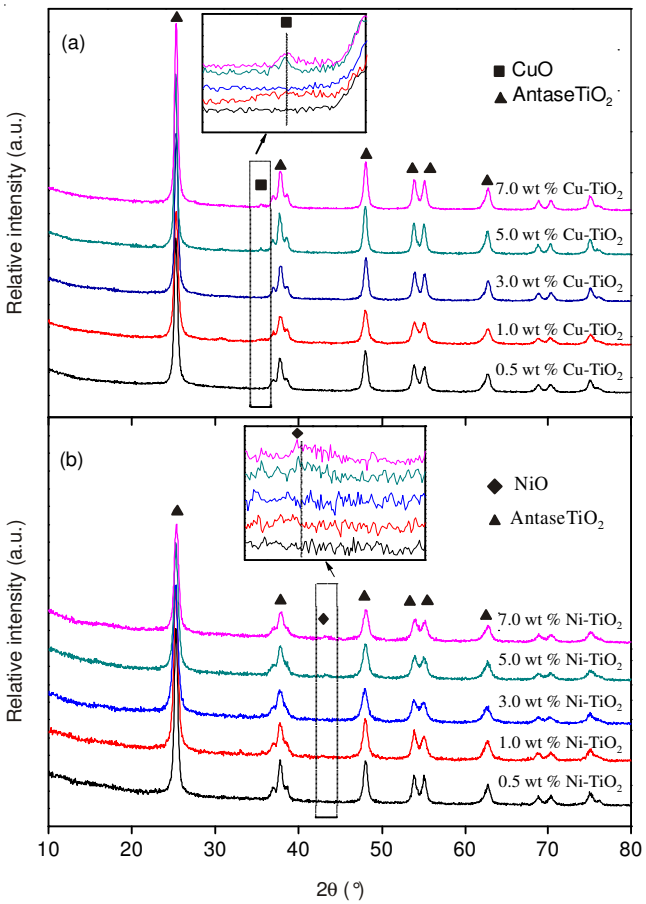

Fig. 1. XRD patterns for (a) Cu-TiO_2 and (b) Ni-TiO_2

The values of crystal size were estimated from the Debye-Scherrer equation, using the anatase (101) reflection. From the Table-1, it can be clearly seen that the grain size of TiO_2 first decreased and then increased with increasing Cu content. This may be because when the dopant amount was low, ionic

Cu might enter the TiO_2 matrix and replace Ti^{4+} lattice sites, enhancing the intergranular cohesion to induce lattice misfit, thus inhibiting direct contact between particles and hindering grain growth[25,26]. However, when the doping content increased to such an extent that some of the Cu ions could not enter the TiO_2 lattice, a coalescence process might occur because sintering is favored by the presence of excessive Cu[27]. Different from Cu-TiO_2, it clearly shows that the crystallite size of the Ni-TiO_2 decreased from 15.5 to 12.3 nm with increasing Ni doping in Table-1. This can be explained by that the existence of Ni^{2+} can inhibit the growth of crystalline size of TiO_2[28].

A weak peak at 35.6º, indexed to CuO, was also observed in the enlarged XRD patterns[29-31] and the relative intensity of this peak increased with increasing Cu doping [inset in Fig. 1(a)]. In addition, a characteristic diffraction peak, corresponding to NiO, was also found at $2\theta = 43.3$º. Its intensity also increased gradually in accord with the increase of the amount of Ni doping[32]. It is conclude that the photocatalysts contain Cu and Ni in the form of bivalent oxides rather than monovalent oxide or zerovalent metal.

The broad-scan XPS spectra of Cu-TiO_2 and Ni-TiO_2 powders, before and after irradiation, are shown in Fig. 2(a). Surface atoms O, Ti, Cu and Ni were observed, together with C atoms originating from the instrument background[33]. From the high-resolution XPS spectra (Fig. 2(b)), the binding energy (BE) peak of O1s was located at 529.8 eV and those of Ti 2p at binding energies 458.5 eV ($2p_{3/2}$) and 464.4 eV ($2p_{1/2}$) [Fig. 2(c)] are in good agreement with spectra showing the presence of typical Ti^{4+} [34-36].

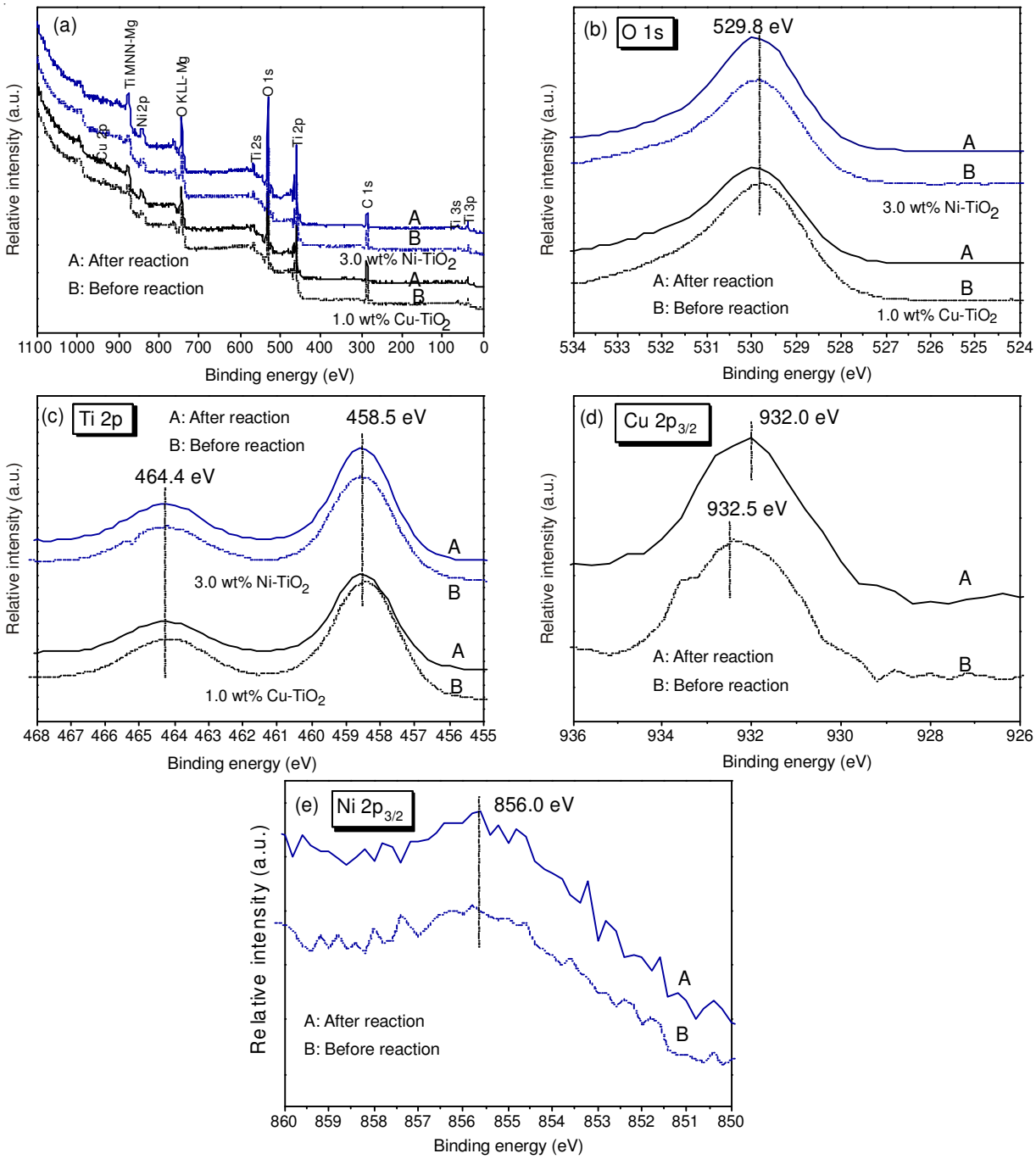

Fig. 2. XPS spectra of (a) 1.0 wt. % Cu-TiO_2 and 3.0 wt. % Ni-TiO_2, together with XPS spectra in the core levels of (b) O 1s, (c) Ti 2p, (d) Cu $2p_{3/2}$ and (e) Ni $2p_{3/2}$

TABLE-1
PROPERTIES OF CATALYSTS

Catalyst	Crystalline phase	S_{BET} (m^2/g)	Particle size (nm)
TiO_2	Anatase	52.00	15.5
0.5 wt. % Cu-TiO_2	Anatase	38.53	15.5
1.0 wt. % Cu-TiO_2	Anatase	40.41	14.9
3.0 wt. % Cu-TiO_2	Anatase	37.88	15.5
5.0 wt. % Cu-TiO_2	Anatase	35.01	17.5
7.0 wt. % Cu-TiO_2	Anatase	29.32	17.5
0.5 wt. % Ni-TiO_2	Anatase	66.99	15.4
1.0 wt. % Ni-TiO_2	Anatase	69.74	13.4
3.0 wt. % Ni-TiO_2	Anatase	72.53	13.4
5.0 wt. % Ni-TiO_2	Anatase	65.98	12.9
7.0 wt. % Ni-TiO_2	Anatase	58.67	12.3

In addition, Fig. 2(d) shows that the Cu $2p_{3/2}$ peak at 932.5 eV has a FWHM of 3.7 eV. The measured BE is higher than reference data for Cu_2O (932.1 eV) but smaller than the value for CuO (933.4 eV) reported by Wagner *et al.* [33,37]. This shift might be attributed to the fact that the surface characteristics of nanoparticles are different from those of the bulk oxides, resulting in the changed oxidation state[30]. Furthermore, some electrons might migrate from TiO_2 to Cu^{2+} due to the interaction between them, causing the negative shift of Cu $2p_{3/2}$[38]. The peak FWHM of 3.7 eV is close to the reported value of 3.4 eV for bulk CuO, suggesting that the copper species is present as Cu^{2+} [39,40].

We could also deduce the oxidation state of Cu from the synthetic method used since no reducing agent was added during the hydrolysis of $Ti(OBu)_4$. Therefore, it is expected that Cu in the precursors will be in the form of $Cu(NO_3)_2$ before thermal treatment since the thermal decomposition of $Cu(NO_3)_2$ at atmospheric pressure in the range 182-312 °C generates CuO, but the formation of Cu_2O requires an increase of temperature to 900 °C[41]. Thus, along with the XRD mearsurements, it is concluded that the Cu^{2+} species is the dominant chemical state of Cu present in the photocatalysts. Our results are consistent with previous observations, where CuO is formed when using $Cu(NO_3)_2$ as the precursor for the preparation of Cu-TiO_2[42-44].

The binding energy value of Ni $2p_{3/2}$ for the nickel oxide species is located at 856.0 eV, as shown in Fig. 2(e). This corresponds closely to the binding energy of NiO (856.0 eV) reported in a previous study[45]. We conclude that the valence state of Ni is +2, which matches the XRD determination very well.

It is suggested that the tiny deviation of the Cu $2p_{3/2}$ peak before and after reaction is the result of reduction of CuO to other species during the photoreduction[29,46]. In contrast, the valence state of Ni remained almost unchanged, since no obvious shift of the peak of Ni $2p_{3/2}$ was observed after 24 h UV illumination.

TEM images of the samples are shown in Fig. 3. It is clear from the mass contrast that the dense particles consist of well dispersed TiO_2. These have irregular shapes, with an average diameter of 10-20 nm. High-resolution TEM (HRTEM) of 1.0 wt. % Cu-TiO_2 and 3.0 wt. % Ni-TiO_2 are shown in the inset of Figs. 3(a) and 3(b), respectively. The obvious lattice fringes with spacings of 0.17 nm and 0.21 nm match well those for the CuO (020) and NiO (002) planes[47,48]. The heterostructural boundary of the catalysts can be clearly seen in the HRTEM image, indicating that the p-type nanoparticles of CuO or NiO are compact and well attached to the n-type TiO_2 surface. In other words, a promising p-n heterojunction photocatalyst, with well designed architecture, has been constructed.

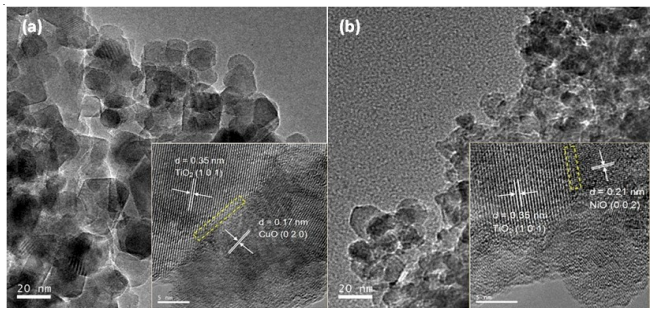

Fig. 3. TEM and HRTEM (inset) images of (a) 1.0 wt. % Cu-TiO_2 and (b) 3.0 wt. % Ni-TiO_2

It is necessary to study the effect of Cu or Ni doping on the surface properties of catalysts. The S_{BET} of the various Cu-TiO_2 and Ni-TiO_2 composite particles are listed in Table-1. It can be seen that the specific surface area of TiO_2 is 52.0 m^2/g, while those of Cu-TiO_2 are smaller ranging from 29.32 to 40.41 m^2/g with a range of Cu content from 0.5 to 7.0 wt. %. This is likely to be because some titania micropores could be blocked by copper doping[49,50]. In contrast, the S_{BET} of Ni-TiO_2 increased with the increase in the amount of doped Ni and then dropped, with a maximum value of 72.53 m^2/g at 3.0 wt. % Ni doping. This is reasonable because Ni doping not only can inhibit the growth of grain and suppress the aggregation of the particles but can also occupy the pores of catalyst particles, like Cu.

The UV-visible absorption spectra of the Cu-TiO_2 and Ni-TiO_2 photocatalysts are depicted in Fig. 4. Strong absorption at 200-305 nm is observed for all the samples. The obvious long-tail absorption in the visible region may be due to extra tail states in the bandgap caused by Cu or Ni doping and the elevation of the baseline is believed to be due to the presence of additional clusters of CuO or NiO[51-54].

Photocatalytic activity of catalysts: The whole photo-reduction process of CO_2 in solution can be separated into several stages from a kinetic point of view[31, 55]. First, CO_2 molecules continuously transfer from the gas phase to the liquid phase. Next, the CO_2 molecules dissolved in solution pass through the phase interfacial transition layer between solution and catalyst and then reach the active site of the photocatalyst. Subsequently, the CO_2 molecules at the active site capture the photogenerated electrons to form CO_2^- anion radicals and then interact with the protons in water to form intermediates or final photoproducts[56]. Finally, the products desorb from the photocatalyst surface to vacate active sites so that the photoreduction of CO_2 can proceed again. Clearly, the CO_2 photoreduction process involves mass transfer, photoelectron generation and transfer and chemical reactions, as well as other surface reactions, such as adsorption and desorption[57].

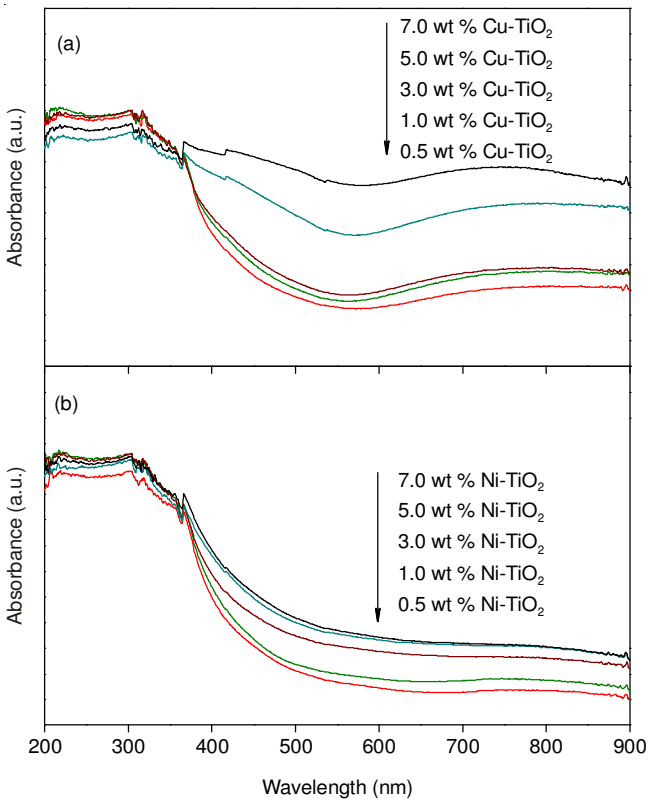

Fig. 4. UV-visible absorption spectra of (a) Cu-TiO_2 and (b) Ni-TiO_2

Control tests consisting of a reaction in the dark with the catalysts and a reaction under UV-light irradiation without catalysts were also carried out in our experiments. No carbon-containing products and H_2 were detectable, suggesting that both the direct photolysis of CO_2 and its adsorption in the dark can be neglected.

The photocatalytic activity of nanostructured Cu-TiO_2 and Ni-TiO_2 composite catalysts for the reduction of CO_2 under UV light irradiation are shown in Fig. 5. In this work, the photocatalytic activity is quantified in terms of the CO_2^- conversion ability (CCA) and light-utilization ability (LUA). The CCA can be indirectly defined as the sum of the number of moles of all independent carbon products produced, including CH_3OH, CO, HCHO and CH_4. In contrast, the LUA evaluates the transformation of the photon and is determined not only by the total quantity of carbon products produced but also by the H_2 yield. Accordingly, the LUA is the sum of the CCA and the H_2 yield. It is clear that either Cu-TiO_2 or Ni-TiO_2 has higher LUA and CCA compared with pure TiO_2 using the same reaction conditions and Ni-TiO_2 exhibits even higher CO_2 conversion than Cu-TiO_2.

The improvement of the LUA over Cu-TiO_2 can be explained by the p-n junction principle[58]. CuO is a p-type semiconductor and TiO_2 belongs to n-type semiconductor. In this investigation, CuO and TiO_2 contact well with each other and form the p-n junction. This gives rise to a space charge region at equilibrium, creating an internal electric field. The internal electric field drives diffusion of the negative charge into the CuO region and the positive charge into the TiO_2

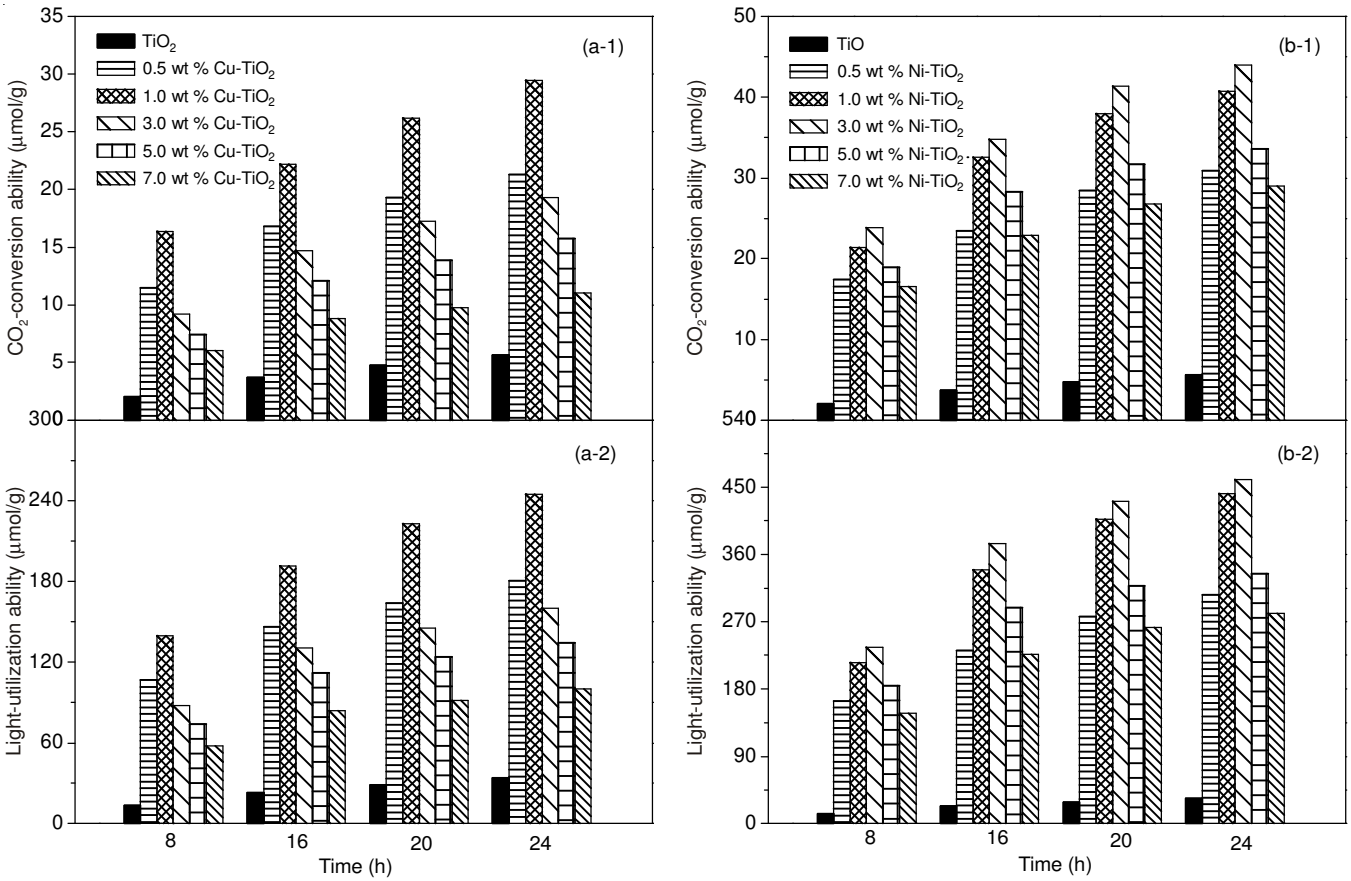

Fig. 5. CO_2-conversion ability and light-utilization ability over the catalysts. (a-1) CCA over Cu-TiO_2, (a-2) LUA over Cu-TiO_2, (b-1) CCA over Ni-TiO_2 and (b-2) LUA over Ni-TiO_2

region. Therefore, once Cu-TiO_2 catalyst is excited by the UV light, the photogenerated electrons will shift naturally into the negative field and holes will move into the positive field, that results in an improved electron and hole separation. In addition, as was just mentioned, due to the role of Cu preferentially coordinating with the π orbital of CO_2, Cu on TiO_2 can effectively accelerate CO_2 activation and reduction *via* the dissociation of the adsorbed CO_2^- [20]. Therefore, Cu doped on TiO_2 can simultaneously increase the adsorption capacity of CO_2 and enhance its subsequent dissociation, finally leading to the substantial improvement of the CO_2 conversion ability.

As with Cu-TiO_2, Choe *et al.*[21] have reported that Ni on TiO_2 coordinates strongly with the $2\pi_\mu \rightarrow 6a_1$ orbital of CO_2. This benefits the dissociation of adsorbed CO_2^- into atomic oxygen and a π-bonded CO fragment, facilitating CO_2 activation and reduction. Additionally, similar to that of Cu-TiO_2 sample, Ni can improve the activity of TiO_2 for CO_2 photoreduction by effectively separating the electrons and holes. This can be understood since NiO and TiO_2 correspond to a p-type and n-type semiconductor, respectively, so they can form a p-n junction and enhance the photocatalytic activity of the Ni-TiO_2[59-61].

Furthermore, it can be seen from Fig. 5 that the CCA and LUA of Cu-TiO_2 catalyst are always smaller than that of the Ni-TiO_2. Apart from the p-n junction behavior, the energy band matching provides additional evidence for the role of the NiO on TiO_2[62]. It is known that the energy of the conduction band (CB) of NiO is -3.06 V (*vs* NHE) higher than TiO_2 and the valence band (VB) of NiO is 0.54 V (*vs* NHE) and is located between E_{CB} (TiO_2) and E_{VB} (TiO_2)[63]. Consequently, after joining NiO and TiO_2 together, the 254 nm UV irradiation causes the photo-excited electrons to flow naturally from the CB of NiO to that of TiO_2, whereas the holes excited in the VB in TiO_2 prefer to flow in the opposite sense to that in NiO. The NiO species acts as an effective hole trap and collector in the reaction system, further suppressing the recombination of excited electron-hole pairs. In this case, electrons, the dominant reducing species remaining in the photocatalysis, react with CO_2 adsorbed on the photocatalyst surface. However, the valence band (VB) and the CB of CuO are at 2.16 V (*vs* NHE) and 0.46 V (*vs* NHE)[64], while those of TiO_2 are at 2.91 V (*vs* NHE) and -0.29 V (*vs* NHE), respectively. Under UV irradiation, the photogenerated e^- and h^+ shift significantly from the CB and VB of TiO_2 to those of the CuO particles and then accumulate in large numbers on the CuO particles, leading to a recombination of the photo-generated electrons and holes.

To evaluate the effects of metal oxide concentration on photocatalytic activity, we carried out a set of tests to photocatalytically reduce CO_2 in water with different weight ratios of Cu/Ti and Ni/Ti. The result of varying the Cu loading from 0.5 to 7.0 wt. % is shown in Fig. 5(a-1) and 5(a-2). The CCA and LUA increased with increasing Cu content up to 1.0 wt. % and then decreased. At the optimum value of 1 %, the CCA and LUA reach the maximum value of 29.43 μmol/g and 244.72 μmol/g, respectively, which is almost seven times that of pure TiO_2 after 24 h UV illumination. Similarly, Figs. 5(b-1) and 5(b-2) show that for the Ni-TiO_2 catalysts, both CCA and LUA for the photocatalytic reaction increase significantly with increasing Ni concentration, up to 3 wt. % and then gradually decrease. In this case, the maximum value of the CCA and LUA, amounting to 43.97 μmol/g and 460.30 μmol/g, respectively, was observed after 24 h UV irradiation, as shown in Figs. 5(b-1) and 5(b-2).

However, the CCA and LUA of the photocatalyst declines with further increase of Cu or Ni content, as shown in Fig. 5. This result can be explained by the fact that photocatalytic reactions occur on the illuminated surface of catalyst. In this study, the BET surface area of Cu-TiO_2 and Ni-TiO_2 dropped as the Cu and Ni doping was further increased. The low surface area is responsible for the low photocatalytic activity due to the creation of less reactive sites on the surface of the photocatalyst. Furthermore, excess CuO and NiO tend to cover the UV-illuminated TiO_2, the absorption of light and generation of electronsholes is reduced, adversely affecting the generation of active electrons for CO_2 photoreduction[65].

Selectivity of photoproducts: A range of catalysts show activities for selective reduction of CO_2 to different photoproducts in aqueous solutions. The major reaction of CO_2 photoreduction can be described by the following equations.

$$\text{Photocatalyst} + h\nu \rightarrow h^+ + e^- \quad (1)$$

$$CO_2 + e^- \rightarrow CO_2^- \quad (2)$$

$$2H^+ + 2e^- \rightarrow H_2 \quad (3)$$

$$CO_2^- + 2H^+ + e^- \rightarrow HCOOH \quad (4)$$

$$CO_2^- + H^+ + e^- \rightarrow CO + OH \quad (5)$$

$$CO_2^- + CO_2 + e^- \rightarrow CO + CO_3^{2-} \quad (6)$$

$$HCOO^- + 2H^+ + e^- \rightarrow HCHO \quad (7)$$

$$HCHO + 2H^+ + 2e^- \rightarrow CH_3OH \quad (8)$$

$$CH_3OH + 2H^+ + 2e^- \rightarrow CH_4 + H_2O \quad (9)$$

Fig. 6 shows the evolution of the photoreduction products of CO_2 in water with Cu-TiO_2 and Ni-TiO_2 as the photocatalyst, respectively. Initially, the amount of products increased rapidly but then slowed with additional photoreduction time. This is the result of adsorption of the intermediate products on the surface of the catalysts, which causes a partial deterioration of the activities of photocatalysts during the photoreduction experiments[66].

Evidently, CO_2 could be selectively photoreduced to CH_4 on Cu-TiO_2 or Ni-TiO_2 photocatalysts. The yields of the products using Cu-TiO_2 followed the order $H_2 > CH_4 > CH_3OH > CO > HCHO$. By comparison, the yields for Ni-TiO_2 followed the order $H_2 > CH_4 > CH_3OH > HCHO > CO$. The standard reduction potential of CO_2/CO, $CO_2/HCHO$, CO_2/CH_3OH and CO_2/CH_4 is -0.53 V, -0.48 V, -0.38 V and -0.24 V, respectively[67,68]. Theoretically, the yield order of CO_2 reduction should be $CH_4 > CH_3OH > H_2 > HCHO > CO$ under stable state. In our experiments, the photocatalytic reduction of CO_2 over Cu-TiO_2 is inconsistent with the order. This is most probably because the photocatalytic system is not under thermodynamic equilibrium within the reaction time.

Conclusion

TiO_2 nanoparticles with a range of Cu or Ni loading were prepared by means of a hydrolysis method and the yields of several kinds of photoproducts in the reduction of CO_2 were investigated in NaOH solution under UV illumination. The metals Cu and Ni are present as CuO and NiO on the surface of TiO_2 and significantly enhanced the photocatalytic activity due to the synergistic combination of dissociation of CO_2 and retarding of the recombination of electron-hole pairs. CO_2 was

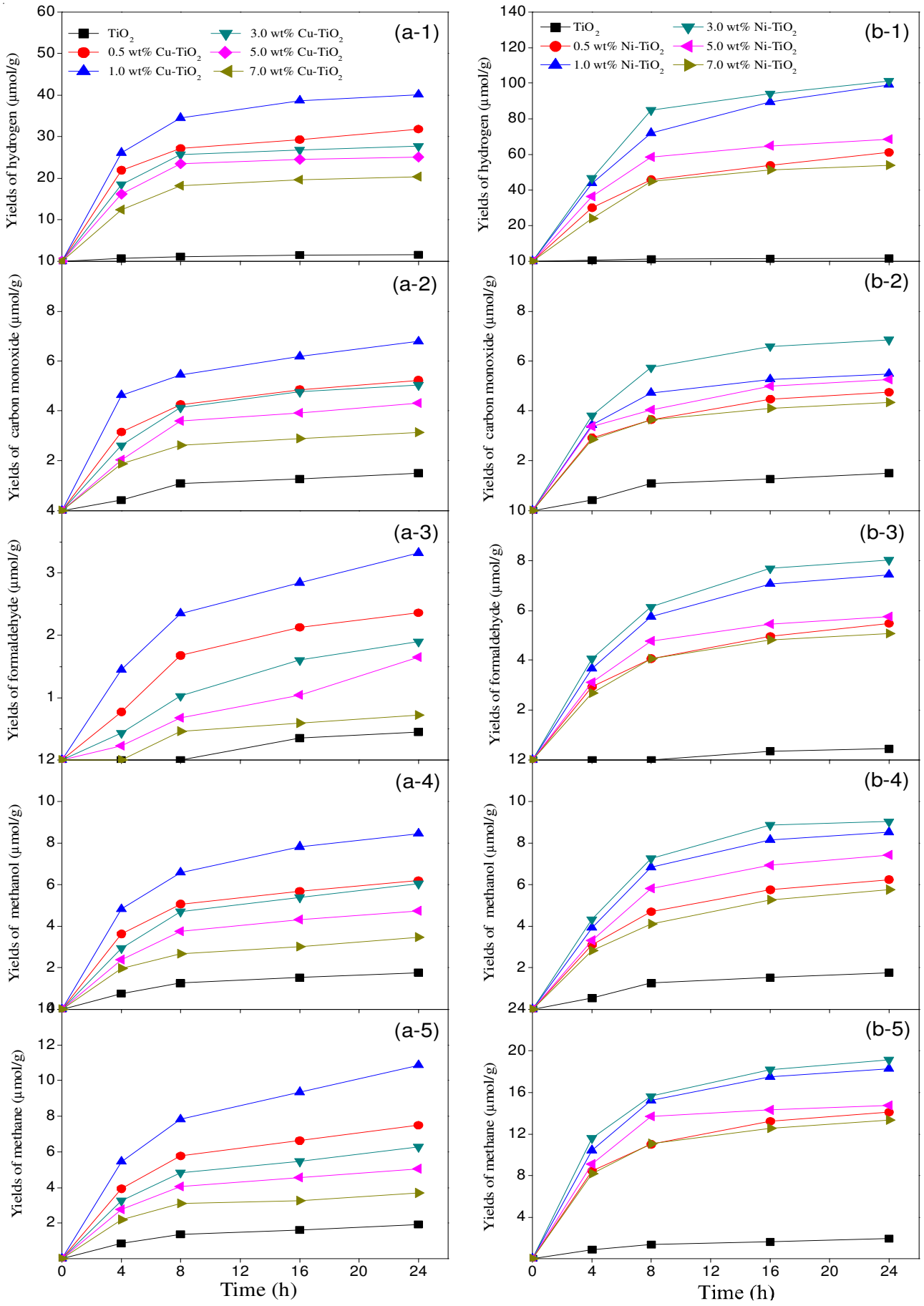

Fig. 6. Time dependence of the yields of products over (a) Cu-TiO_2 and (b) Ni-TiO_2 catalysts

selectively transformed to a number of compounds such as CO, HCHO and CH_4. Ni-TiO_2 has superior photocatalytic activity compared with Cu-TiO_2 due to the presence of a p-n junction and matching band potentials. CH_4 was identified as the major product using Cu-TiO_2 or Ni-TiO_2 as the photocatalyst. An in-depth study of the activity and selectivity of other photocatalysts is still required.

ACKNOWLEDGEMENTS

This work was supported by the National Natural Science Foundation of China (21177115 and 21076196) and the Zhejiang Provincial Natural Science Foundation of China (LR13B070002).

REFERENCES

1. H. Takeda and O. Ishitani, *Coord. Chem. Rev*., **254**, 346 (2010).
2. Q.Y. Sun, Y.J. Jiang, Z.Y. Jiang, L. Zhang, X.H. Sun and J. Li, *Ind. Eng. Chem. Res*., **48**, 4210 (2009).
3. Y. Kohno, H. Hayashi, S. Takenaka, T. Tanaka, T. Funabiki and S. Yoshida, *J. Photochem. Photobiol. Chem*., **126**, 117 (1999).
4. Q.H. Zhang, W.D. Han, Y.J. Hong and J.G. Yu, *Catal. Today*, **148**, 335 (2009).
5. J.C.S. Wu, *Catal. Surv. Asia*, **13**, 30 (2009).
6. Y. Bessekhouad, D. Robert and J.V. Weber, *J. Photochem. Photobiol. Chem*., **163**, 569 (2004).
7. G. Rothenberger, D. Fitzmaurice and M. Graetzel, *J. Phys. Chem*., **96**, 5983 (1992).
8. L.M. Sun, X. Zhao, X.F. Cheng, H.G. Sun, Y.L. Li, P. Li and W.L. Fan, *Langmuir*, **28**, 5882 (2012).
9. J.G. Yu, T.T. Ma and S.W. Liu, *Phys. Chem. Chem. Phys*., **13**, 3491 (2011).
10. D. Uner and M.M. Oymak, *Catal. Today*, **181**, 82 (2012).
11. J.C. Wu, T.H. Wu, T. Chu, H.J. Huang and D.P. Tsai, *Top. Catal*., **47**, 131 (2008).
12. N. Sasirekha, S.J.S. Basha and K. Shanthi, *Appl. Catal. B*, **62**, 169 (2006).
13. Y. Kohno, T. Yamamoto, T. Tanaka and T. Funabiki, *J. Mol. Catal. Chem*., **175**, 173 (2001).
14. R.S. Sonawane and M.K. Dongare, *J. Mol. Catal. Chem*., **243**, 68 (2006).
15. S.B. Zhang, J.K. Wang and X.L. Wang, *J. Nat. Gas Chem*., **17**, 179 (2008).
16. I.H. Tseng, W.C. Chang and J.C.S. Wu, *Appl. Catal. B*, **37**, 37 (2002).
17. B.J. Liu, T. Torimoto and H. Yoneyama, *J. Photochem. Photobiol. Chem*., **115**, 227 (1998).
18. S.T. Hussain, K. Khan and R. Hussain, *J. Nat. Gas Chem*., **18**, 383 (2009).
19. Q.Y. Zhang, Y. Li, E.A. Ackerman, M. Gajdardziska-Josifovska and H. Li, *Appl. Catal. A*, **400**, 195 (2011).
20. L.J. Liu, C.Y. Zhao and Y. Li, *J. Phys. Chem. C*, **116**, 7904 (2012).
21. S.J. Choe, H.J. Kang, D.H. Park, D.S. Huh and J. Park, *Appl. Surf. Sci*., **181**, 265 (2001).
22. X.L. Ding, V. Pagan, M. Peressi and F. Ancilotto, *Mater. Sci. Eng. C*, **27**, 1355 (2007).
23. Z.Y. Wang, H.C. Chou, J.C.S. Wu, D.P. Tsai and G. Mul, *Appl. Catal. A*, **380**, 172 (2010).
24. M.L. Bruce, R.P. Lee and M.W. Stephens, *Environ. Sci. Technol*., **26**, 160 (1992).
25. A.S. Deshpande, D.G. Shchukin, E. Ustinovich, M. Antonietti and R.A. Caruso, *Adv. Funct. Mater*., **15**, 239 (2005).
26. N. Venkatachalam, M. Palanichamy, B. Arabindoo and V. Murugesan, *J. Mol. Catal. Chem*., **266**, 158 (2007).
27. J.F. Zhu, W. Zheng, B. He, J.L. Zhang and M. Anpo, *J. Mol. Catal. Chem*., **216**, 35 (2004).
28. M.A. Ahmed, *J. Photochem. Photobiol. A*, **238**, 63 (2012).
29. H. Nasution, E. Purnama, S. Kosela and J. Gunlazuardi, *Catal. Commun*., **6**, 313 (2005).
30. K.V.R. Chary, G.V. Sagar, D. Naresh, K.K. Seela and B. Sridhar, *J. Phys. Chem. B*, **109**, 9437 (2005).
31. X.Y. Yang, T.C. Xiao and P.P. Edwards, *Int. J. Hydrogen Energy*, **36**, 6546 (2011).
32. H.J. Seo and E.Y. Yu, *J. Ind. Eng. Chem*., **3**, 85 (1997).
33. B.F. Xin, P. Wang, D.D. Ding, J. Liu, Z.Y. Ren and H.G. Fu, *Appl. Surf. Sci*., **254**, 2569 (2008).
34. B.M. Reddy, B. Chowdhury, I. Ganesh, E.P. Reddy, T.C. Rojas and A. Fernández, *J. Phys. Chem. B*, **102**, 10176 (1998).
35. B.M. Reddy, B. Chowdhury, E.P. Reddy and A. Fernández, *J. Mol. Catal. Chem*., **162**, 431 (2000).
36. N.L.V. Carreño, I.T.S. Garcia, L.S.S.M. Carreño, M.R. Nunes, E.R. Leite, H.V. Fajardo and L.F.D. Probst, *J. Phys. Chem. Solids*, **69**, 1897 (2008).
37. C.D. Wagner, W.M. Riggs, L.E. Davis and J.F. Moulder, Handbook of X-Ray Photoelectron Spectroscopy, Perkin-Elmer Corporation, Minnesota (1979).
38. S. Rengaraj and X.Z. Li, *J. Mol. Catal. Chem*., **243**, 60 (2006).
39. T. Ghodselahi, M.A. Vesaghi, A. Shafiekhani, A. Baghizadeh and M. Lameii, *Appl. Surf. Sci*., **255**, 2730 (2008).
40. J.Y. Park, Y.S. Jung, J. Cho and W.K. Choi, *Appl. Surf. Sci*., **252**, 5877 (2006).
41. I.V. Morozov, K.O. Znamenkov, Y.M. Korenev and O.A. Shlyakhtin, *Thermochim. Acta*, **403**, 173 (2003).
42. J. Bandara, C.P.K. Udawatta and C.S.K. Rajapakse, *Photochem. Photobiol. Sci*., **4**, 857 (2005).
43. B. Xu, L. Dong and Y. Chen, J. Chem. Soc., *Faraday Trans*., **94**, 1905 (1998).
44. S.Y. Qin, F. Xin, Y.D. Liu, X.H. Yin and W. Ma, *J. Colloid Interf. Sci*., **356**, 257 (2011).
45. S.B. Zhang, J.K. Wang and X.L. Wang, *J. Nat. Gas Chem*., **17**, 179 (2008).
46. Y. Li, W.N. Wang, Z.L. Zhan, M.H. Woo, C.Y. Wu and P. Biswas, *Appl. Catal. B*, **100**, 386 (2010).
47. P. Umek, M. Pregelj, A. Gloter, P. Cevc, Z. Jaglicic, M. Ceh, U. Pirnat and D. Arcon, *J. Phys. Chem. C*, **112**, 15311 (2008).
48. X.Y. Song, Y.X. He, C.M. Lampert, X.F. Hu and X.F. Chen, *Sol. Energy Mater. Sol. Cells*, **63**, 227 (2000).
49. J.C.S. Wu, I.H. Tseng and W.C. Chang, *J. Nanopart. Res.*, **3**, 113 (2001).
50. J. Zhao and X.D. Yang, *Build. Environ*., **38**, 645 (2003).
51. I.H. Tseng and J.C.S. Wu, *Catal. Today*, **97**, 113 (2004).
52. P.A. Forsh, A.G. Kazanskii, H. Mell and E.I. Terukov, *Thin Solid Films*, **383**, 251 (2001).
53. K.K. Chattopadhyay, J. Dutta, S. Chaudhuri and A.K. Pal, *Diamond Rel. Mater.*, **4**, 122 (1995).
54. M. Epifani, C. Giannini, L. Tapfer and L. Vasanelli, *J. Am. Ceram. Soc*., **83**, 2385 (2000).
55. N.M. Dimitrijevic, B.K. Vijayan, O.G. Poluektov, T. Rajh, K.A. Gray, H.Y. He and P. Zapol, *J. Am. Chem. Soc*., **133**, 3964 (2011).
56. P. Usubharatana, D. McMartin, A. Veawab and P. Tontiwachwuthikul, *Ind. Eng. Chem. Res*., **45**, 2558 (2006).
57. C.C. Lin, W.T. Liu and C.S. Tan, *Ind. Eng. Chem. Res*., **42**, 2381 (2003).
58. J.F. Zhang, Y.G. Yang and W. Liu, *Int. J. Photoenergy*, **2012**, 139739 (2012).
59. C. Shifu, Z. Sujuan, L. Wei and Z. Wei, *J. Hazard. Mater*., **155**, 320 (2008).
60. C.J. Chen, C.H. Liao, K.C. Hsu, Y.T. Wu and J.C.S. Wu, *Catal. Commun*., **12**, 1307 (2011).
61. S. Liu, X.P. Liu, Y.S. Chen and R.Y. Jiang, *J. Alloys Comp*., **506**, 877 (2010).
62. J. Bandara and H. Weerasinghe, *Sol. Energy Mater. Sol. Cells*, **85**, 385 (2005).
63. X.Y. Wu and E.K.L. Yeow, *Chem. Commun.*, **46**, 4390 (2010).
64. Y. Xu and M.A.A. Schoonen, *Am. Mineral*., **85**, 543 (2000).
65. D. Chen and E.H. Jordan, *J. Sol-Gel Sci. Technol*., **50**, 44 (2009).
66. N. Sasirekha, S.J.S. Basha and K. Shanthi, *Appl. Catal. B*, **62**, 169 (2006).
67. S.C. Roy, O.K. Varghese, M. Paulose and C.A. Grimes, *ACS Nano*, **4**, 1259 (2010).
68. W. Shin, S.H. Lee, J.W. Shin, S.P. Lee and Y.S. Kim, *J. Am. Chem. Soc*., **125**, 14688 (2003).